Molecular Therapy
Nucleic Acids
Original Article

Fine and Predictable Tuning of TALEN Gene Editing Targeting for Improved T Cell Adoptive Immunotherapy

Anne-Sophie Gautron,[1,3] Alexandre Juillerat,[2,3] Valérie Guyot,[1] Jean-Marie Filhol,[1] Emilie Dessez,[1] Aymeric Duclert,[1] Philippe Duchateau,[1] and Laurent Poirot[1]

[1]Cellectis SA, 8 Rue de la Croix Jarry, 75013 Paris, France; [2]Cellectis Inc., 430E 29th Street, New York, NY 10016, USA

Using a TALEN-mediated gene-editing approach, we have previously described a process for the large-scale manufacturing of "off-the-shelf" CAR T cells from third-party donor T cells by disrupting the gene encoding TCRα constant chain (*TRAC*). Taking advantage of a previously described strategy to control TALEN targeting based on the exclusion capacities of non-conventional RVDs, we have developed highly efficient and specific nucleases targeting a key T cell immune checkpoint, PD-1, to improve engineered CAR T cells' functionalities. Here, we demonstrate that this approach allows combined *TRAC* and *PDCD1* TALEN processing at the desired locus while eliminating low-frequency off-site processing. Thus, by replacing few RVDs, we provide here an easy and rapid redesign of optimal TALEN combinations. We anticipate that this method can greatly benefit multiplex editing, which is of key importance especially for therapeutic applications where high editing efficiencies need to be associated with maximal specificity and safety.

INTRODUCTION

Recent advancement in genome-engineering technology is changing the landscape of biological research, especially for the development of new therapeutic applications. This groundbreaking technology provides scientists with novel opportunities to develop new methodologies to ask and answer critical questions. This advancement is highlighted by the increased use of programmable DNA-binding agents such as transcription activator-like effector (TALE) and RNA-guided CRISPR/CRISPR-associated (Cas) systems that became part of the most powerful gene-editing tools.[1–3] These novel and robust DNA-targeting platforms allow a wide use of gene manipulation in both research and the development of novel therapies. These engineered enzymes can introduce DNA double-strand breaks (DSBs) with high efficiency and specificity into desired target sequences, and their ability to precisely cleave a specific locus is being used to disrupt genes via mutagenic non-homologous end joining (NHEJ).

Adoptive immunotherapy is a new paradigm for treating cancer. Recent reports have highlighted the synergistic possibilities of genome editing and the chimeric antigen receptor (CAR) T cell technology to develop the next generation of therapeutic applications. Although CAR-engineered T cells infiltrate the tumor tissue and persist over long periods,[4] tumor reduction is frequently transient mainly due to tumor-associated immune repression. The latter is mediated, at least in part, by regulatory T cells (Tregs), which heavily infiltrate solid tumor lesions, and by the upregulation of multiple immune-checkpoint molecules (CTLA-4, PD-1, LAG3, or TIM-3) on tumor-infiltrating lymphocytes. Immune checkpoint pathways strongly downregulate T cell activation, carrying the important function of keeping nascent T cell responses in check and reducing the likelihood of an immune attack against normal tissues. During tumorigenesis, however, cancer cells may exploit these co-inhibitory pathways to resist detection or avoid elimination by the adaptive immune system.[5] The PD-1 checkpoint pathway is thought to act primarily in peripheral tissues to dampen ongoing immune responses and/or to prevent damage to self-tissues. The ability of non-immune cells to express ligands for PD-1 such as PD-L1 is exploited by tumors as a way to avoid immune attack.[6,7] Preliminary clinical findings with blockers of immune-checkpoint proteins such as CTLA-4 and PD-1 indicate broad and diverse opportunities to enhance anti-tumor immunity with the potential to produce durable clinical responses.[8–13] However, most tissues rely on PD-L1 expression to limit T cell responses.[14] Thus, the systemic administration of PD-L1/PD-1-blocking antibodies carries a risk of breaking peripheral tolerance, which might lead to autoimmune responses. Recent studies have demonstrated the feasibility and potency of approaches incorporating advanced gene-editing technologies into adoptive cell therapy protocols to silence immune checkpoints as a strategy to overcome locally active immune escape pathways.[15,16] We have previously described a platform for the production of "off-the-shelf" CAR T cells (UCAR T cells) from unrelated third-party donor T cells by disrupting TCRα constant gene *TRAC*.[17] By combining the beneficial effects of

Received 25 May 2017; accepted 11 October 2017;
https://doi.org/10.1016/j.omtn.2017.10.005.

[3]These authors contributed equally to this work.

Correspondence: Anne-Sophie Gautron, Cellectis SA, 8 Rue de la Croix Jarry, 75013 Paris, France.
E-mail: anne-sophie.gautron@cellectis.com
Correspondence: Philippe Duchateau, Cellectis SA, 8 Rue de la Croix Jarry, 70513 Paris, France.
E-mail: philippe.duchateau@cellectis.com

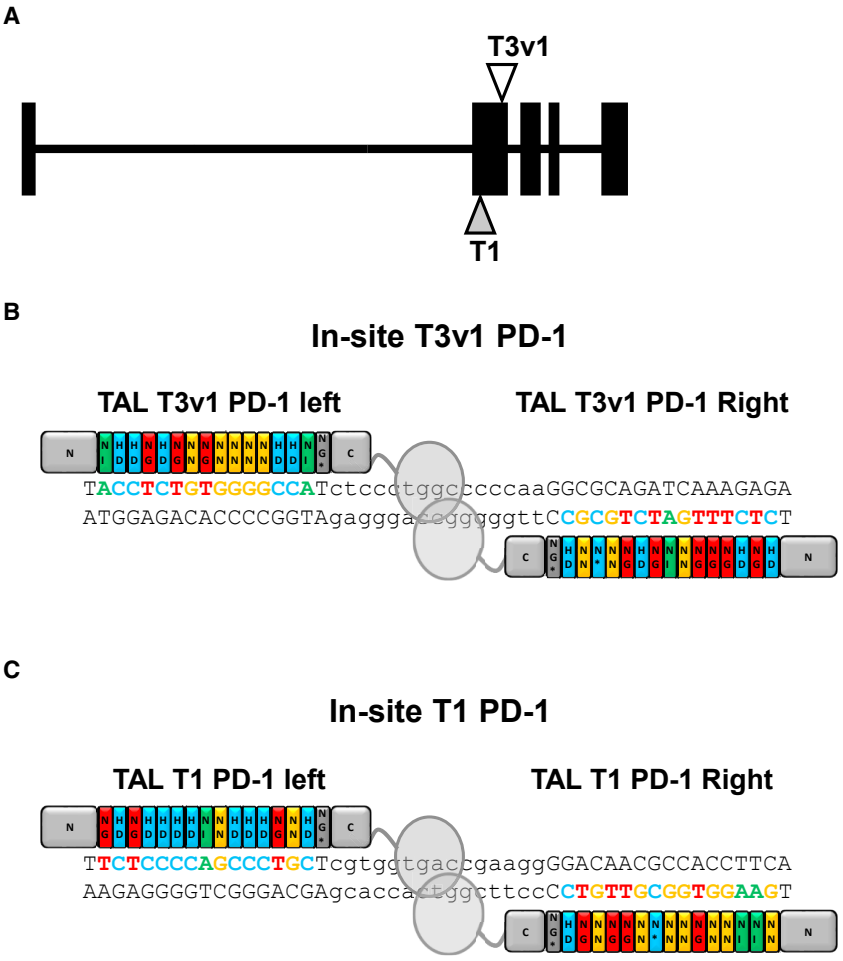

Figure 1. Design of Two PD-1 TALEN Targeting the First Exon of *PDCD1* Locus

(A) Schematic representation of the *PDCD1* (PD-1) genomic sequence. Black boxes represent exons, and triangles represent the approximate TALEN-binding sites. (B and C) Schematic representations of the loci and T3v1 (B) and T1 (C) PD-1 TALEN used to knock out *PDCD1* in primary T cells.

both PD-1 blockade and CAR therapy, we have not only reduced the effective cost of this adoptive immune therapy but also simplified the protocol of administration as compared to a therapy that would combine the injection of both UCAR T cells and anti-PD-1 antibody.

Here, we used the latest in the transcription activator-like effector nuclease (TALEN) technology to develop highly efficient and specific nucleases targeting a key T cell immune checkpoint, PD-1, to improve engineered CAR T cells' functionalities. By taking advantage of unique features of the TALE DNA targeting, its modularity, associated with the independence of the targeting modules, we aimed at replacing natural targeting modules, the repeat variable diresidues (RVDs), with appropriately chosen non-conventional RVDs (RVDs not found in the natural repertoires of TALE) to improve the specificity of targeting for multiplex genome editing. Our results demonstrate that our strategy based on exclusion properties of these non-conventional RVDs allowed combined *TRAC* and *PDCD1* TALEN processing at the desired locus while eliminating low-frequency off-site processing. These results further confirmed previous reports showing that strategies replacing a few RVDs allowed the easy and rapid redesign of optimal TALEN nuclease combinations (so-called multiplex editing),[18–20] a feature of prime importance especially for therapeutic applications where high editing efficiencies associated with maximal specificity and safety is of prime importance.

RESULTS

PDCD1 Locus Is Efficiently Processed Using TALEN T3v1

Today, four RVDs are mainly implemented and used, NI, HD, NN, and NG, to target an adenine, a cytosine, a guanine, and a thymine, respectively. Using features from our TALEN scaffold (TAL DNA binding array of 15.5 RVDs and spacer length of 15 base pairs) we designed and synthesized 2 TALEN T3v1 and T1 (first version of TALEN design) targeting the second exon of the *PDCD1* locus where the PD-L1 binding site is located (Figures 1A–1C). For more clarity throughout this manuscript, the term TALEN represents the nuclease entity composed of two engineered TALE fused to the FokI catalytic domain. In order to evaluate the efficiency of our TALEN, we performed targeted mutagenesis experiments at the *PDCD1* locus. Thirteen days post-mRNA electroporation, PD-1 production was assessed on non-transfected or TALEN-transfected T cells by flow cytometry after exclusion of non-viable cells (Figure 2A). PD-1 production is strongly disrupted on the surface of T3v1-transfected T cells as compared to non-transfected T cells (Figure 2A, left panels). Indeed, the surface detection is reduced by about 65% (from 4.6% to 1.6%) after mRNA TALEN transfection. As demonstrated in the literature, PD-1 is one of the key-inhibitory receptor expressed by activated T cells, and its expression is upregulated following antigen- and ligand-receptor engagement.[21] Thus, PD-1 production increases early after activation and decreases about a week after the initial activation. By reactivating non-transfected T cells, PD-1 is markedly re-induced at their surface, while its production remains very low without additional reactivation. Indeed, PD-1 is only detected on 4.6% of non-transfected T cells 17 days after their initial activation, while we observe a frequency of 72.2% of PD-1$^+$ T cells 3 days after reactivation (Figure 2B, left panels). We observe a reduction of about 85% (from 72.2% to 9.3%) when T3v1-transfected T cells were reactivated. Even though our second available TALEN to knock out *PDCD1* (T1) is efficient at processing *PDCD1* locus, its efficiency remains lower than T3v1 TALEN (Figure 2B, right panels).

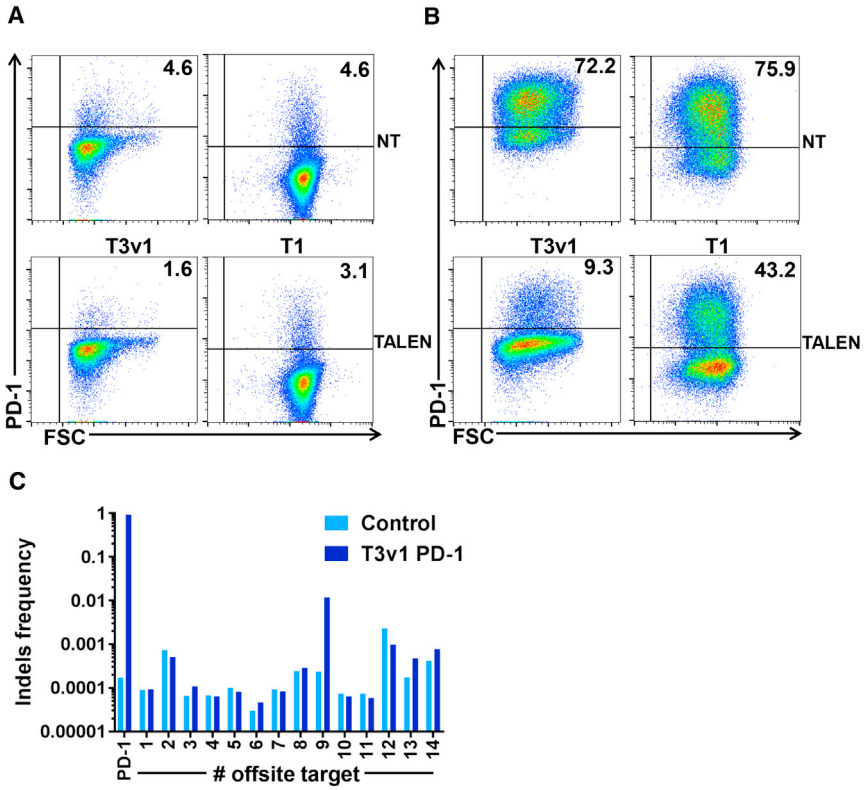

Figure 2. T3v1 PD-1 TALEN Is Highly Efficient to Disrupt *PDCD1* Gene Expression in Primary T Cells

Four days after activation, 5 million T cells were transfected with 10 μg of each mRNA encoding the left and right arms of T3v1 or T1 PD-1 TALEN. Ten days after transfection, T cells were reactivated (B) or not (A) using Dynabeads human T activator CD3/CD28. Three days later, PD-1 production was assessed by flow cytometry on viable non-transfected (NT) T cells (upper panels) and transfected (TALEN) T cells (bottom left panels corresponding to T3v1 and right panels to T1) using PD-1 monoclonal antibody (mAb) in combination with a live/dead cell marker. The frequency of positive cells is indicated in each panel. Dot plots are representative of at least three independent experiments. (C) The efficiency of TALEN-mediated gene processing was analyzed by high-throughput DNA sequencing analysis of engineered T cell genomic DNA harvested 6 days after transfection. Potential in-site and off-site targets were carefully evaluated for these loci.

Indeed, PD-1 surface detection on T1-transfected and -reactivated T cells is reduced by 43% (from 75.9% down to 43.2% after reactivation). T3v1 TALEN being our lead candidate, we characterized in depth by high-throughput DNA sequencing (454 method) the molecular events generated by this TALEN at its target locus. Genomic DNA, recovered from T cells grown for more than 6 days after electroporation of PD-1 TALEN was used to generate specific PCR amplicons. Our sequencing results reveal insertion/deletion (indel) frequencies of ~70% to 80% at the locus of interest for T3v1 TALEN (Figure 2C), confirming that TALEN-mediated processing of *PDCD1* gene is very highly efficient under our experimental conditions. We also characterized in depth the molecular events generated by this TALEN at potential off-site targets. These off-site targets were systematically defined as genomic sequences bearing any combinations of TALEN binding sites containing ≤ 4 mismatches with respect to the sequence to target and separated from one another by 9 to 30 bp. The lists of potential off-site targets were generated and scored taking into account the nature and position of the substitutions as described previously.[22] The 14 (T3v1) targets with the highest scores regardless of their genomic position, as well as the top four targets located in (or within 200 bp from) a coding sequence, were chosen for high-throughput DNA sequencing analysis. One off-site target (v1OS9) is found to be processed at low frequency (>2 orders of magnitude lower than the in-site, 0.5%) for T3v1 TALEN, the other sites tested do not show mutagenesis above background (Figure 2C). All together, these data confirm the possibility to design TALEN that present very high levels of activity on their cognate in-site target while sparing potential off-site targets.

The Use of Non-conventional RVDs Improves Targeting Specificity in the Context of a Single Knockout

Considering the very high efficiency of the T3v1 TALEN at the desired *PDCD1* locus, we decided to investigate whether we could modify this TALEN using non-conventional RVDs to maintain the same high level of activity at the desired locus but completely prevent the TALEN activity at the identified off-site sequence.[18] The OS9 detected is mostly probably due to a homodimer association of the left half TALEN T3v1. Using the same strategy as previously presented,[18] we first identified the mismatches between the in-site and off-site binding sequences. Then we identified non-conventional RVDs that allow discrimination at the mismatch position, between the in-site and the off-site nucleotides. To narrow the choice of non-conventional RVDs, we focused on non-conventional RVDs that will present minimal (or preferably no) relaxed specificities for the two remaining nucleotides to prevent any new off-site targeting. We further favored modification in the first half of the TALE array since this portion of the TALE array has previously been shown to have a higher impact on the targeting specificity.[22,23] Thus, after having identified the mismatches between the in-site and off-site binding sequences of the left arm of the TALEN, we designed two new TALEN (v2 and v3) by incorporating two non-conventional RVDs at the position 1 and 2 (T3v2) and 1 and 9 (T3v3) (Figure 3A). In these specific examples, NI and HD were replaced by GN and QD, respectively (T3v2) or NI and NN were replaced by GN and GR (T3v3). We then investigated the activity and specificity of both TALEN T3v2 and v3. As shown by flow cytometry, PD-1 surface detection after T cell reactivation is reduced by 87% (from 50.2% down to 6.5%; T3v2) and 74% (from 50.2% down to 13%; T3v3). These

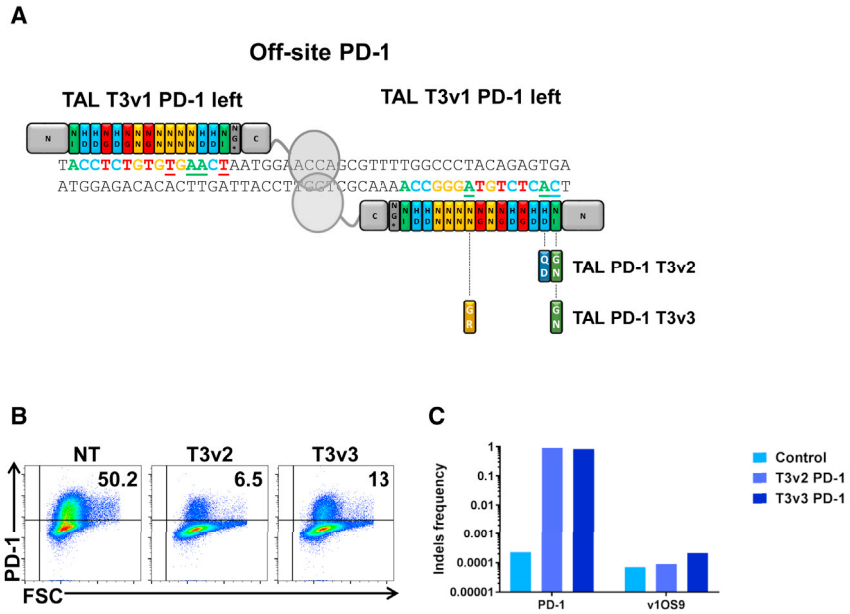

Figure 3. T3v2 and T3v3 PD-1 TALEN Are as Efficient as T3v1 PD-1 TALEN at Disrupting *PDCD1* Gene Expression in Primary T Cells and Do Not Induce Mutagenesis at the Off-Site Sequence Tested

Four days after activation, 5 million T cells were transfected with 10 μg of each mRNA encoding the left and right arms of TALEN T3v2 or T3v3 PD-1. (A) Schematic representation of the locus targeted by a homodimer left of the T3v1 PD-1 TALEN and of the new TALEN used in the primary T cell target discrimination experiment.[18] (B) Nine days post-transfection, T cells were reactivated using Dynabeads human T activator CD3/CD28. Two days later, surface PD-1 was measured by flow cytometry on viable non-transfected T cells (left panel) and transfected (T3v2 and T3v3) T cells (middle and right panels) using PD-1 mAb in combination with a live/dead cell marker. The frequency of positive cells is indicated in each panel. Dot plots are representative of at least three independent experiments. (C) The efficiency of TALEN-mediated gene processing was analyzed by high-throughput DNA sequencing analysis of engineered T cell genomic DNA harvested 6 days after transfection. Potential in-site and off-site 9 targets were carefully evaluated for these loci.

efficiencies of PD-1 TALEN activities are very similar to the efficiency of T3v1 PD-1 TALEN. Having demonstrated that a very high activity of PD-1 TALEN was maintained at the in-site locus, we further investigated the capacity of the new TALEN to process the previously defined off-site 9 (v1OS9) target. As expected from the phenotypic results obtained (Figure 3B) our sequencing results reveal indel frequencies of ~80% to 90% at the locus of interest, confirming that TALEN-mediated processing of *PDCD1* gene by T3v2 and T3v3 PD-1 TALEN are highly efficient. More importantly, the v1OS9 tested does not show mutagenesis above background level (Figure 3C), indicating that our strategy to improve TALEN specificity by replacing conventional RVDs with non-conventional RVDs is highly efficient.

The Use of Non-conventional RVDs Improves Targeting Specificity in the Context of a Double Knockout

To align with the allogeneic approach we developed,[17,24] we combined both TRAC and T3v2 PD-1 TALEN. We then characterized in depth by high-throughput DNA sequencing the molecular events generated by those two TALEN at their respective target loci and their potential off-site targets. In this particular example, the two TALEN were designed separately to present individual optimal (high in-site and no or low off-site processing) activities, without taking into account the possibility of a simultaneous use (multiplex gene editing) in their respective design. To analyze the activity profile of the combined two TALEN, we further increased the number of analyzed off-sites to the 25 targets with the highest scores. This allowed us to also include the first 10 ranked targets that would be the result of the combination of one of each arm of the two TALEN (PD-1 and TRAC) used (Figure 4A). The sequencing results reveal high indel frequencies at both loci of interest (*PDCD1* and *TRAC*), demonstrating that TALEN-mediated processing of *PDCD1* and *TRAC* gene is highly efficient. Nevertheless, 2.9% of indels are detected at one of the highest ranked off-sites studied, the v2OS3, which corresponds to an off-site induced by a heterodimer TRAC left/PD-1 left. Using the same design strategy, we elaborated one new TALEN T3v4 by replacing the first and seventh RVDs by non-conventional RVDs. By design, we chose a combination of non-conventional RVDs; NI and NN were replaced by KL and YK, respectively. That would allow preventing processing of the previously identified v1OS9 and the newly identified v2OS3. We focus our TALEN re-engineering efforts on the PD-1 left arm, as the number and type of mismatches observed with the TRAC left arm were expected to be already more impactful on the TALEN activity. We thus investigated the specificity and activity of each of these new TALEN as compared to T3v1 PD-1 original TALEN. As shown by an overlay analysis of PD-1 production on the surface of reactivated cells, we observed a similar reduction of surface PD-1 for T cells transfected with each of the different PD-1 TALEN (Figure 4B). We then monitored the capacity of the new TALEN to edit the previously defined off-site targets v1OS9 (due to the homodimer association) and v2OS3 (due to the heterodimer association). In this experiment, we obtain indel frequencies of ~70% to 80% at the *PDCD1* locus and ~60% at the *TRAC* locus (Figure 4C). As expected, the v1OS9 tested does not show mutagenesis above background level for any of the new TALEN tested, and the v2OS3 tested does not show mutagenesis above background for the last T3v4 PD-1 TALEN produced (Figure 4C), indicating that our strategy to improve TALEN specificity by replacing conventional RVDs with non-conventional RVDs is highly efficient and can be translated to prevent off-site processing while maintaining high levels of activity at the different in-site loci. Importantly, as expected, the other potential off-site targets that were previously

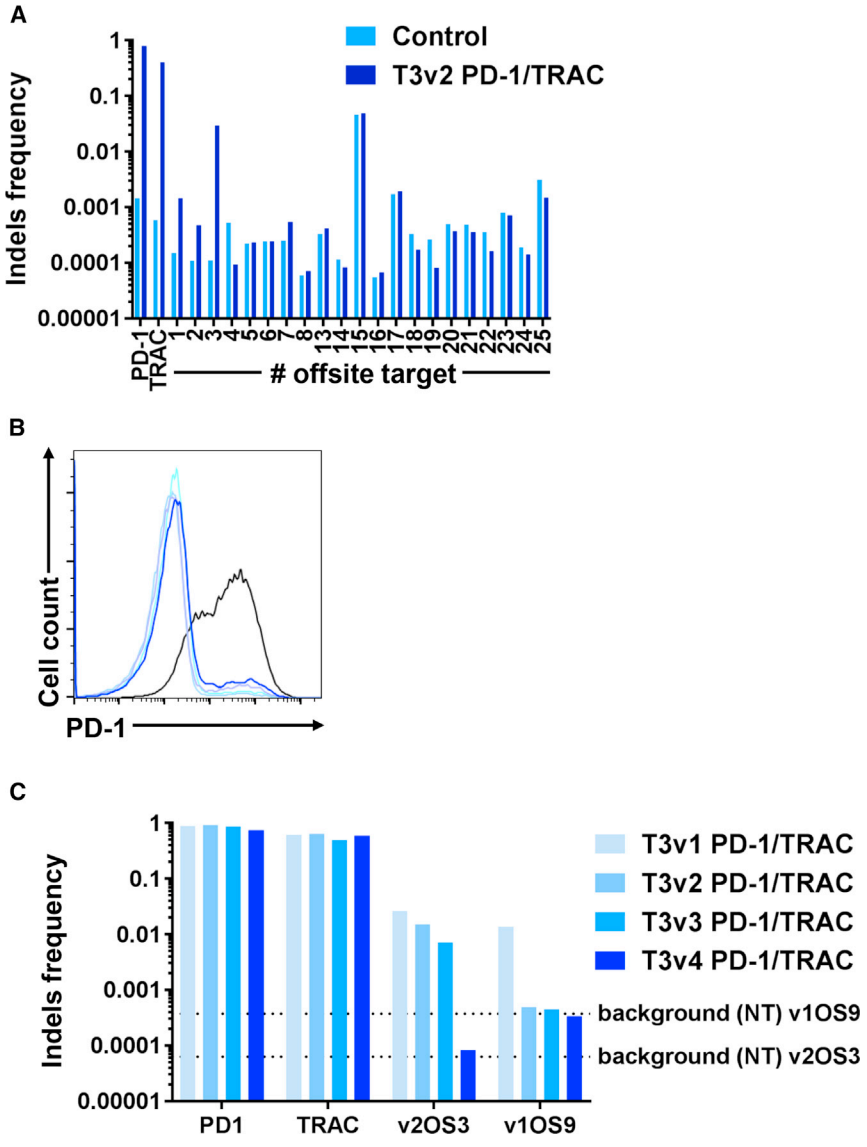

Figure 4. T3v4 PD-1 TALEN Is as Efficient as T3v1 PD-1 TALEN at Disrupting *PDCD1* Gene Expression in Primary T Cells and Does Not Induce Mutagenesis at the Off-Site Sequences Tested

Four days after activation, 5 million T cells were transfected with 10 μg of each mRNA encoding the left and right arms of TALEN T3v2 PD-1 (A) or TALEN T3v1, T3v2, T3v3, or T3v4 (B and C) in combination with 10 μg of each mRNA encoding the left and right arms of TALEN TRAC. (A) The efficiency of TALEN-mediated gene processing was analyzed by high-throughput DNA sequencing analysis of engineered T cell genomic DNA harvested 6 days after transfection. Potential in-site and off-site targets were carefully evaluated for these loci. The off-site OS9, OS10, OS11, and OS12 have identical potential TALEN binding sites as the OS8. The PCR products generated for deep-sequencing analysis for OS8, OS9, OS10, OS11, and OS12 are more than 99.8% identical. Thus, OS8 represents the pooled data of the off-sites mentioned above. (B) Nine days after transfection, T cells were reactivated using Dynabeads human T activator CD3/CD28. Two days later, the mean fluorescence intensity (MFI) of surface PD-1 detection was assessed by flow cytometry on viable non-transfected T cells and transfected T cells using PD-1 mAb in combination with a live/dead cell marker. Histograms are representative of at least two independent experiments. (C) The efficiency of TALEN-mediated gene processing was analyzed by high-throughput DNA sequencing analysis of engineered T cell genomic DNA harvested 6 days after transfection. Potential in-site and off-site 9 and off-site 3 targets were carefully evaluated for these loci.

studied were unaffected (no processing) by the incorporation of the non-conventional RVDs.

PDCD1 and *TRAC* Double Knockout CAR T Cells Are Highly Efficient to Eliminate Target Cells *In Vitro*

Having demonstrated that the *PDCD1* locus could be efficiently edited using TALEN, containing or not non-conventional RVDs, we further investigated whether the *in vitro* cytolytic activity was affected by the double knockout of *PDCD1* and *TRAC*. T cells were transduced or not with lentiviral particles encoding CD20 CAR and transfected or not with mRNA encoding T3v4 PD-1 and TRAC TALEN. The efficiencies of transduction and transfection were assessed by flow cytometry 4 days after transduction. When transduced at a MOI of 5, more than 60% of the cells express CD20 CAR on their surface (Figure 5A, left panels), while surface PD-1 is reduced by almost 50% when CAR T cells are transfected with mRNA encoding T3v4 PD-1 TALEN (Figure 5A, middle panels). As observed in Figure 5A, PD-1 surface detection on CAR T cells is higher compared to that on CAR negative T cells (middle versus right columns), reflecting the activation level of T cells. These observations are in accordance with previous studies that demonstrated that PD-1 is not detected on resting T cells but is inducibly re-induced within 24 h after stimulation, the highest level of expression being reached 2 to 4 days after activation.[21,25] These two sets of T cells (wild-type [WT] and dual *PDCD1*/*TRAC* knockout) were then challenged in an *in vitro* long-term cytotoxicity assay using target cells presenting the CAR antigen. As anticipated, we observed that independently of the ratio of T cells and target cells, the dual knockout CAR T cells are at least as efficient as WT CAR T cells at eradicating the targets cells *in vitro* (Figure 5B). At a ratio of 1:20 (T cell:target cell), 64% of the target cells are killed in co-culture with WT CAR T cells, while 68.3% are eliminated in co-culture with *PDCD1* knockout CAR T cells. At a ratio of 1:10, the cytotoxic activity of WT CAR T cells toward their specific antigen reaches 82%, while it reaches 84.8% for *PDCD1* knockout

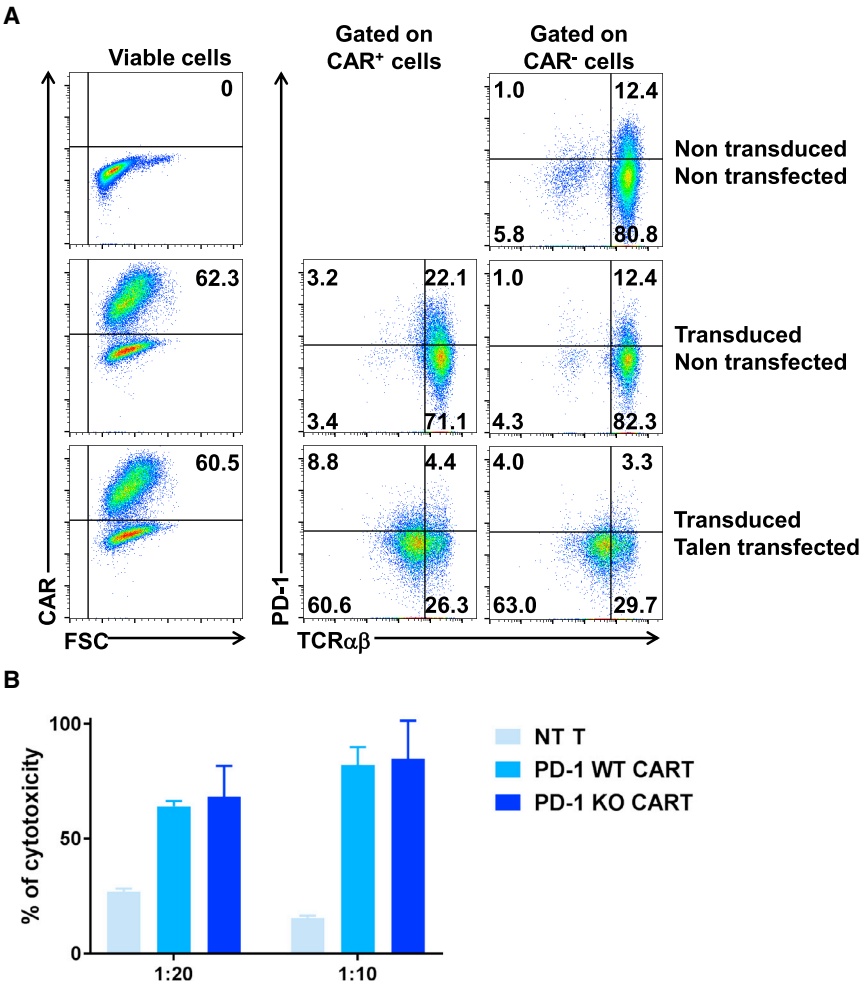

Figure 5. The *In Vitro* Anti-tumor Activity of *PDCD1* Knockout CAR T Cells Is at Least as Efficient as the Activity of *PDCD1* WT CAR T Cells

CD20 CAR T cells were transfected or not with 10 μg of each mRNA encoding the left and right arms of TALEN T3v4 PD-1 in combination with TRAC TALEN. (A) Transduction and transfection efficiencies were assessed 4 days post-transduction on viable T cells using PD-1 and TCRαβ mAb, and CAR expression was reflected by the level of BFP expression. (B) The effect of *PDCD1* knockout on the CAR T cells toward antigen-presenting cells over-expressing PD-L1 was assessed in a flow-based cytotoxicity assay. The $CD20^+$ and $CD20^-$ target cell viability was measured after 3 days of co-culture with engineered CAR T cells at ratio set to 1:20 and 1:10 effector:target. Data are shown as mean ± SD of triplicates per point of two independent experiments.

CAR T cells. All together, these data demonstrate that the dual knockout of the *PDCD1* and *TRAC* genes is not impacting the cytolytic properties of CAR T cells.

The study we present here reports the fine and precise "multilayer" genome editing of primary T cells. Such reengineering of the TALEN DNA binding motives allows the reliable serial and sequential generation of precise designer nucleases from already existing TALEN. In particular, we demonstrated that the UCAR T cell (*TRAC* knockout CAR T cell) platform can be further rapidly, efficiently, and safely engineered using TALEN containing non-conventional RVDs. The multiplexed engineered UCAR T cells (*TRAC* and *PDCD1* knockout) maintained a potent *in vitro* anti-tumor function. Different recent studies have demonstrated that the disruption of PD-1 on CAR T cells enhanced the anti-tumor activity *in vitro* and in animal models.[15,16,26,27] Beyond our proof-of-concept study, further additional *in vitro* and *in vivo* experiments will be desirable to fully assess the benefits of such multiplex engineered UCAR T cells with adequate tumor models.

DISCUSSION

One of the major challenge of gene editing using designer nuclease, especially for clinical applications, is the risk that off-target cleavage can occur at sequences within the genome that contain a few mismatches related to the targeted sequence of interest. Thus, the possibility to control and finely tune the targeting specificity of such platforms represents a key issue. Regarding TALEs, the DNA-binding domain consists of highly conserved 33–35 amino acid sequence repeats with divergent 12th and 13th amino acids in each repeat.[28,29] These so-called RVDs are highly variable and show a strong correlation with specific nucleotide recognition. So far, four DNA targeting modules (RVDs) have been used by most researchers (NI, HD, NN, and NG), but these naturally found RVDs only explore about 5% of the possible diversity repertoire at these two key positions.[30,31] Using this four-RVD repertoire, TALEN has already proven to be specific and compatible to *ex vivo* engineering of primary T cells for therapeutic applications with no or very low (background) levels of off-site processing.[17] Specificity of targeting being a key factor, especially for therapeutic application, the use of the NN canonical RVD to target a guanine was questioned due to its ability to target both an adenine and a guanine.[28,29] Several research groups have therefore studied the implementation of alternative natural RVDs, such as NK and NH to improve the specificity of guanine targeting.[30,31] Recent studies took advantage of the vast repertoire offered by DNA-targeting characteristics of RVDs (positions 12 and 13), to identify and characterize new non-conventional RVDs with novel intrinsic targeting specificity features.[18–20] This strategy to exclude the targeting of specific genomic sequences (so-called off-site targets) by TALEN is based on the unique targeting properties of non-conventional RVDs. In particular, the mapping of their binding properties (affinity for the different nucleotides) revealed that the nature of the amino acid at position 13 of these

non-conventional RVDs largely defined the base preference (as already observed for canonical RVDs)[28,29,32–35] with some effects on the affinity. The identity of the amino acid at position 12 was described to be the major contributor to the RVD binding strength (with possible minimal effect on specificity). In addition, studies on the sensitivity of TALE array to epigenetic modifications (e.g., 5-methylcytosine) highlighted how steric hindrance between the amino acids at positions 12 and 13 and the targeted nucleotide is affecting the recognition and binding of an RVD array to its target sequence.[36,37] The overall better understanding of the interaction between the RVD array and the targeted sequence allowed the implementation of such non-conventional RVDs, improving the discrimination between different nucleotides and therefore further increasing the specificity of TALE-based molecular tools.[18–20]

Better mastering the targeting properties (e.g., specificity) of designer nuclease is of prime interest for clinical application, as demonstrated, for example, by the synergy that could be obtained between gene editing and adoptive immunotherapies (e.g., CAR T cells) developed to fight cancer.[17,38] The current optimized version of our process is initiated by CD3-dependent T cell activation at time 0, incorporates a transduction step at 72 hr to allow for the expression of a CAR, and finally concludes with a TALEN mRNA electroporation step for *TRAC*/*CD52* gene disruption at 120 hr. Subsequent to the TALEN electroporation step, the cells are cultured in a closed system for 10 to 12 days followed by magnetic depletion of remaining TCRαβ-positive cells. Using this process, TCR/CD52-deficient CAR T cells were manufactured with highly reproducible yields. Since there will not be any possibility to deplete PD-1$^+$ cells because of the lack of good manufacturing practice (GMP) magnetic depletion system for PD-1, the TALEN that induces the highest level of knockout was chosen. In such a case where a TALEN is highly efficient but one off-site target is found to be processed even though at low frequency, it is extremely useful to have the possibility to design TALEN that maintain such high levels of activity on their cognate in-site target while sparing the potential off-site target.

CAR T cells have demonstrated significant responses in patients with treatment-refractory hematologic malignancies but have only modest results in solid tumors. This is likely due to a host of hurdles encountered in the tumor microenvironment of solid tumors,[39,40] especially intrinsic inhibitory pathways mediated by upregulated inhibitory receptors such as PD-1 reacting with their cognate ligand within the tumor. Many studies have demonstrated that advanced-generation human CAR T cells are reversibly inactivated within the solid tumor microenvironment.[41] Thus, PD-1 pathway antagonism can augment human CAR T cell function.[42,43] Recently, we and others underlined that disruption of endogenous *PDCD1* using designer nuclease enhances the efficacy of gene-disrupted CAR T cell therapy or the function of tumor-reactive T cells used for adoptive cell transfer (ACT) in tumor models.[15,26,27] However, disrupting PD-1 expression on CAR T cells that could eventually express autoreactive T cells might lead to autoimmune adverse events such as those described with systemic PD-1 antibody blockade. Here, we implemented the non-conventional RVD approach to edit the genome of human primary T cells with TALEN presenting improved discrimination between the desired on-site and the off-sites targets. We previously described a platform for the production of "off-the-shelf" CAR T cells from unrelated third-party donor T cells by disrupting TCRα constant gene *TRAC*.[17] We therefore focused on optimizing a TALEN targeting the *PDCD1* locus that can be used in combination with the previously reported TRAC TALEN, such a multiplex genome-editing strategy could allow the generation of highly potent and tumor-specific UCAR T cells and prevent the risk of adverse events previously observed.[8] By incorporating non-conventional RVDs on the left T3v1 PD-1 half TALEN, we were able to produce an optimized and highly efficient TALEN that is not processing the low-frequency PD-1 off-sites identified with first generations of TALEN (for use of the PD-1 TALEN alone or simultaneously with the TRAC TALEN). In this study, we decided to use simultaneously two TALEN pairs that were designed separately. In such case, the combination of arms of the different TALEN may lead to the targeting of off-site sequences that were not taken into account in the original TALEN design. The *a posteriori* strategy of educated TALEN reengineering that we presented here can be further broadly adapted to multiplex TALEN gene editing. All together, these results showed that a very fine and predictable tuning of a TALEN targeting can be obtained by incorporating a few non-conventional RVDs. This approach could positively impact the development of new generations of treatments involving gene editing for many diseases. Whether the identification of potential off-sites is performed *in silico* or experimentally, once the evaluation of genomic toxicity is performed during clinical trials, the detection of off-target mutagenesis could block further development of a candidate product. Here, our approach enables fine tuning of the TALEN used to abrogate off-target activity specifically where it is detected. In addition, one can imagine combining this approach with the use of engineered obligated heterodimeric FokI cleavage domains[44–46] to prevent the pairing of the specific half TALEN molecules responsible for off-site activity. Moreover, we demonstrated that the *in vitro* anti-tumor activity of *PDCD1* knockout CAR T cells is not impaired. This development validated in human primary T cells will enable TALEN tools for gene editing to be applied more broadly and safely in basic research and disease treatment.

MATERIALS AND METHODS

Antibodies

The following monoclonal antibodies and reagents were used: for surface staining, anti-PD-1 (clones PD1.3.1.3 and EH12.2H7 from Miltenyi Biotech and Biolegend, respectively), anti-TCRαβ (clone BW242/412 from Miltenyi Biotech), and fixable viability dye eFluor 780 from eBioscience. All the cytometry analyses were performed on a FACSCanto II (BD Biosciences).

Cell Culture

Frozen peripheral blood mononuclear cells (PBMC) were obtained from healthy volunteer donors (Allcells). T lymphocytes were activated directly from PBMCs using Dynabeads human T activator

CD3/CD28 (Invitrogen), taking into account the frequency of $CD3^+$ cells at a ratio of 1:1 bead:cell. Activated T cells were then immediately diluted in X-Vivo-15 (Lonza) media supplemented by 20 ng/mL IL-2 (final concentration) (Miltenyi Biotech) and 5% human serum AB (Seralab). Jeko-PD-L1 (ATCC-CRL3006) were generated by lentiviral transduction with an expression cassette for PD-L1. PD-$L1^+$ cells were single cell sorted by high-speed flow cytometry on a SH800 (Sony) at a purity >98%. Jeko and Jeko-PD-L1 were cultured in RPMI 1640 containing Glutamax (Gibco) supplemented by 20% fetal bovine serum (FBS) (Lonza), 100 U/mL Penicillin, and 100 µg/mL Streptomycin (Lonza).

TALEN

TRAC, T3v1 PD-1, T3v2 PD-1, T3v3 PD-1, and T3v4 PD-1 TALEN were obtained from Cellectis. The target sequences for each TALEN were as follows:

TRAC: 5′-TTGTCCCACAGATATCCagaaccctgaccctgCCGTGTACCAGCTGAGA-3′

PDCD1: 5′-TACCTCTGTGGGGCCATctccctggcccccaaGGCGCAGATCAAAGAGA-3′

Two 17-bp recognition sites (upper case letters) are separated by a 15-bp spacer.

mRNA

mRNAs were synthesized using the mMessage mMachine T7 Ultra Kit (Life Technologies). RNAs were purified with RNeasy columns (QIAGEN) and eluted in cytoporation medium T (Harvard Apparatus). Following process optimization, TALEN mRNAs were produced by a commercial manufacturer (Trilink Biotechnologies).

Cell Transfection and Investigation of Knockout Efficiency

Four to five days after activation, T cells were transfected with 10 µg of each mRNA encoding the left and right arms of TALEN. Transfection was performed using Agilpulse technology. Cells were then immediately diluted in X-Vivo-15 media supplemented by 20 ng/mL IL-2 (final concentration) and 5% human serum AB. Transfected T cells were eventually diluted at 1×10^6 cells/mL and kept in culture at 37°C in the presence of 5% CO_2 and 20 ng/mL IL-2 (final concentration) and 5% human AB serum for further characterization.

Nine days post-transfection, T cells were reactivated or not using Dynabeads human T activator CD3/CD28 at a bead:cell ratio of 0.5:1. Three days later, production of PD-1 at the membrane was assessed by flow cytometry. Knockout efficiencies can be investigated by flow cytometry starting from day 2 post-transfection, but *PDCD1* knockout is more easily detected after reactivation.

Cell Transduction

Three days after activation, 6×10^6 primary T cells resuspended in 3.6 mL of X-Vivo-15 media were cultured in a T25 flask pre-coated by 30 µg/mL of Retronectine in the presence of lentiviral particles to obtain a multiplicity of infection of 5. After 2 hr of incubation at 37°C, 3 mL of complete media 2X (X-vivo-15, 10% AB serum, and 40 ng/mL IL-2) was added to the cellular suspension. After overnight incubation, cells were washed, resuspended in a complete media at 1×10^6 cells/mL, and passaged every 2 or 3 days.

CARs

Second-generation CD20 CAR was constructed using single-chain antibody fragments derived from antibody clones C230H, hinge and transmembrane regions from CD8A, intracellular domain from TNFRSF9 (CD137), and intracellular domain from CD247 (CD3ζ). The single-chain variable fragment (scFv) is preceded by the sequence encoding the blue fluorescent protein (BFP), which will reflect the expression of the CAR. CD20 CAR was cloned into a commercial lentiviral vector backbone downstream of an EF1a promoter, and concentrated lentiviral vectors were produced by Vectalys (Toulouse, France).

Mutagenesis Analysis

PCR amplifications spanning *TRAC* or *PDCD1* targets or *in silico* predicted potential off-site targets were performed from gDNA harvested 6 days post-transfection using primers described in the Supplemental Materials and Methods. Purified PCR products were sequenced using the Illumina method (Miseq 2x250 nano V2) or 454 sequencing system (454 Life Sciences). At least 2,065 sequences were obtained per PCR product for Illumina and 1,364 for 454, and sequences were analyzed for the presence of site-specific mutations. The total number of reads, the total number of events detected, and the estimated indel frequencies are summarized in the Supplemental Materials and Methods.

Cytotoxicity Assay

The cytolytic activity of *PDCD1* WT or *PDCD1* knockout engineered T cells endowed with CD20 CAR was assessed using a flow cytometry-based cytotoxicity assay. In this assay, target cells presenting the CAR target antigen (Jeko or Jeko PD-L1) as well as control cells not presenting the CAR target antigen were labeled with CellTrace carboxyfluorescein succinimidyl (CFSE; Life Technologies). The target cell populations were co-incubated at 37°C at different ratios of engineered effector CAR T cells (effector/target) of 1:20 and 1:10 for 3 days in a final volume of 200 µL of culture medium corresponding to the culture medium of the target cell line. After 3 days, the whole cell population was recovered, washed in PBS, labeled with eFluor 780 viability marker (eBioscience), and target cell viability was assessed by flow cytometry.

SUPPLEMENTAL INFORMATION

Supplemental Information includes Supplemental Materials and Methods and can be found with this article online at https://doi.org/10.1016/j.omtn.2017.10.005.

AUTHOR CONTRIBUTIONS

A.-S.G. and A.J. designed and performed the experiments, analyzed data, and wrote the manuscript. A.-S.G. and A.J. contributed equally

to this work. V.G., E.D., and J.-M.F. performed experiments. A.D. analyzed the data. P.D. and L.P. supervised the study and wrote the manuscript.

CONFLICTS OF INTEREST

All coauthors are present Cellectis employees.

REFERENCES

1. Scharenberg, A.M., Duchateau, P., and Smith, J. (2013). Genome engineering with TAL-effector nucleases and alternative modular nuclease technologies. Curr. Gene Ther. *13*, 291–303.
2. Gersbach, C.A., and Perez-Pinera, P. (2014). Activating human genes with zinc finger proteins, transcription activator-like effectors and CRISPR/Cas9 for gene therapy and regenerative medicine. Expert Opin. Ther. Targets *18*, 835–839.
3. Niu, J., Zhang, B., and Chen, H. (2014). Applications of TALENs and CRISPR/Cas9 in human cells and their potentials for gene therapy. Mol. Biotechnol. *56*, 681–688.
4. Till, B.G., Jensen, M.C., Wang, J., Chen, E.Y., Wood, B.L., Greisman, H.A., Qian, X., James, S.E., Raubitschek, A., Forman, S.J., et al. (2008). Adoptive immunotherapy for indolent non-Hodgkin lymphoma and mantle cell lymphoma using genetically modified autologous CD20-specific T cells. Blood *112*, 2261–2271.
5. Pardoll, D.M. (2012). The blockade of immune checkpoints in cancer immunotherapy. Nat. Rev. Cancer *12*, 252–264.
6. Jadus, M.R., Natividad, J., Mai, A., Ouyang, Y., Lambrecht, N., Szabo, S., Ge, L., Hoa, N., and Dacosta-Iyer, M.G. (2012). Lung cancer: a classic example of tumor escape and progression while providing opportunities for immunological intervention. Clin. Dev. Immunol. *2012*, 160724.
7. Zou, W., and Chen, L. (2008). Inhibitory B7-family molecules in the tumour microenvironment. Nat. Rev. Immunol. *8*, 467–477.
8. Topalian, S.L., Hodi, F.S., Brahmer, J.R., Gettinger, S.N., Smith, D.C., McDermott, D.F., Powderly, J.D., Carvajal, R.D., Sosman, J.A., Atkins, M.B., et al. (2012). Safety, activity, and immune correlates of anti-PD-1 antibody in cancer. N. Engl. J. Med. *366*, 2443–2454.
9. Brahmer, J.R., Tykodi, S.S., Chow, L.Q., Hwu, W.J., Topalian, S.L., Hwu, P., Drake, C.G., Camacho, L.H., Kauh, J., Odunsi, K., et al. (2012). Safety and activity of anti-PD-L1 antibody in patients with advanced cancer. N. Engl. J. Med. *366*, 2455–2465.
10. Leach, D.R., Krummel, M.F., and Allison, J.P. (1996). Enhancement of antitumor immunity by CTLA-4 blockade. Science *271*, 1734–1736.
11. Wolchok, J.D., Kluger, H., Callahan, M.K., Postow, M.A., Rizvi, N.A., Lesokhin, A.M., Segal, N.H., Ariyan, C.E., Gordon, R.A., Reed, K., et al. (2013). Nivolumab plus ipilimumab in advanced melanoma. N. Engl. J. Med. *369*, 122–133.
12. Curran, M.A., Montalvo, W., Yagita, H., and Allison, J.P. (2010). PD-1 and CTLA-4 combination blockade expands infiltrating T cells and reduces regulatory T and myeloid cells within B16 melanoma tumors. Proc. Natl. Acad. Sci. USA *107*, 4275–4280.
13. Hodi, F.S., O'Day, S.J., McDermott, D.F., Weber, R.W., Sosman, J.A., Haanen, J.B., Gonzalez, R., Robert, C., Schadendorf, D., Hassel, J.C., et al. (2010). Improved survival with ipilimumab in patients with metastatic melanoma. N. Engl. J. Med. *363*, 711–723.
14. Pen, J.J., Keersmaecker, B.D., Heirman, C., Corthals, J., Liechtenstein, T., Escors, D., Thielemans, K., and Breckpot, K. (2014). Interference with PD-L1/PD-1 co-stimulation during antigen presentation enhances the multifunctionality of antigen-specific T cells. Gene Ther. *21*, 262–271.
15. Menger, L., Sledzinska, A., Bergerhoff, K., Vargas, F.A., Smith, J., Poirot, L., Pule, M., Hererro, J., Peggs, K.S., and Quezada, S.A. (2016). TALEN-mediated inactivation of PD-1 in tumor-reactive lymphocytes promotes intratumoral T-cell persistence and rejection of established tumors. Cancer Res. *76*, 2087–2093.
16. Ren, J., Zhang, X., Liu, X., Fang, C., Jiang, S., June, C.H., and Zhao, Y. (2017). A versatile system for rapid multiplex genome-edited CAR T cell generation. Oncotarget *8*, 17002–17011.
17. Poirot, L., Philip, B., Schiffer-Mannioui, C., Le Clerre, D., Chion-Sotinel, I., Derniame, S., Potrel, P., Bas, C., Lemaire, L., Galetto, R., et al. (2015). Multiplex genome-edited T-cell manufacturing platform for "off-the-shelf" adoptive T-cell immunotherapies. Cancer Res. *75*, 3853–3864.
18. Juillerat, A., Pessereau, C., Dubois, G., Guyot, V., Maréchal, A., Valton, J., Daboussi, F., Poirot, L., Duclert, A., and Duchateau, P. (2015). Optimized tuning of TALEN specificity using non-conventional RVDs. Sci. Rep. *5*, 8150.
19. Miller, J.C., Zhang, L., Xia, D.F., Campo, J.J., Ankoudinova, I.V., Guschin, D.Y., Babiarz, J.E., Meng, X., Hinkley, S.J., Lam, S.C., et al. (2015). Improved specificity of TALE-based genome editing using an expanded RVD repertoire. Nat. Methods *12*, 465–471.
20. Yang, J., Zhang, Y., Yuan, P., Zhou, Y., Cai, C., Ren, Q., Wen, D., Chu, C., Qi, H., and Wei, W. (2014). Complete decoding of TAL effectors for DNA recognition. Cell Res. *24*, 628–631.
21. Chemnitz, J.M., Parry, R.V., Nichols, K.E., June, C.H., and Riley, J.L. (2004). SHP-1 and SHP-2 associate with immunoreceptor tyrosine-based switch motif of programmed death 1 upon primary human T cell stimulation, but only receptor ligation prevents T cell activation. J. Immunol. *173*, 945–954.
22. Juillerat, A., Dubois, G., Valton, J., Thomas, S., Stella, S., Maréchal, A., Langevin, S., Benomari, N., Bertonati, C., Silva, G.H., et al. (2014). Comprehensive analysis of the specificity of transcription activator-like effector nucleases. Nucleic Acids Res. *42*, 5390–5402.
23. Meckler, J.F., Bhakta, M.S., Kim, M.S., Ovadia, R., Habrian, C.H., Zykovich, A., Yu, A., Lockwood, S.H., Morbitzer, R., Elsäesser, J., et al. (2013). Quantitative analysis of TALE-DNA interactions suggests polarity effects. Nucleic Acids Res. *41*, 4118–4128.
24. Valton, J., Guyot, V., Marechal, A., Filhol, J.M., Juillerat, A., Duclert, A., Duchateau, P., and Poirot, L. (2015). A multidrug-resistant engineered CAR T cell for allogeneic combination immunotherapy. Mol. Ther. *23*, 1507–1518.
25. Xing, K., Gu, B., Zhang, P., and Wu, X. (2015). Dexamethasone enhances programmed cell death 1 (PD-1) expression during T cell activation: an insight into the optimum application of glucocorticoids in anti-cancer therapy. BMC Immunol. *16*, 39.
26. Rupp, L.J., Schumann, K., Roybal, K.T., Gate, R.E., Ye, C.J., Lim, W.A., and Marson, A. (2017). CRISPR/Cas9-mediated PD-1 disruption enhances anti-tumor efficacy of human chimeric antigen receptor T cells. Sci. Rep. *7*, 737.
27. Ren, J., Liu, X., Fang, C., Jiang, S., June, C.H., and Zhao, Y. (2017). Multiplex genome editing to generate universal CAR T cells resistant to PD1 inhibition. Clin. Cancer Res. *23*, 2255–2266.
28. Moscou, M.J., and Bogdanove, A.J. (2009). A simple cipher governs DNA recognition by TAL effectors. Science *326*, 1501.
29. Boch, J., Scholze, H., Schornack, S., Landgraf, A., Hahn, S., Kay, S., Lahaye, T., Nickstadt, A., and Bonas, U. (2009). Breaking the code of DNA binding specificity of TAL-type III effectors. Science *326*, 1509–1512.
30. Cong, L., Zhou, R., Kuo, Y.C., Cunniff, M., and Zhang, F. (2012). Comprehensive interrogation of natural TALE DNA-binding modules and transcriptional repressor domains. Nat. Commun. *3*, 968.
31. Streubel, J., Blücher, C., Landgraf, A., and Boch, J. (2012). TAL effector RVD specificities and efficiencies. Nat. Biotechnol. *30*, 593–595.
32. Deng, D., Yan, C., Pan, X., Mahfouz, M., Wang, J., Zhu, J.K., Shi, Y., and Yan, N. (2012). Structural basis for sequence-specific recognition of DNA by TAL effectors. Science *335*, 720–723.
33. Gao, H., Wu, X., Chai, J., and Han, Z. (2012). Crystal structure of a TALE protein reveals an extended N-terminal DNA binding region. Cell Res. *22*, 1716–1720.
34. Mak, A.N., Bradley, P., Cernadas, R.A., Bogdanove, A.J., and Stoddard, B.L. (2012). The crystal structure of TAL effector PthXo1 bound to its DNA target. Science *335*, 716–719.
35. Stella, S., Molina, R., Yefimenko, I., Prieto, J., Silva, G., Bertonati, C., Juillerat, A., Duchateau, P., and Montoya, G. (2013). Structure of the AvrBs3-DNA complex provides new insights into the initial thymine-recognition mechanism. Acta Crystallogr. D Biol. Crystallogr. *69*, 1707–1716.
36. Flade, S., Jasper, J., Gieß, M., Juhasz, M., Dankers, A., Kubik, G., Koch, O., Weinhold, E., and Summerer, D. (2017). The N6-position of adenine is a blind spot for

TAL-effectors that enables effective binding of methylated and fluorophore-labeled DNA. ACS Chem. Biol. *12*, 1719–1725.

37. Valton, J., Dupuy, A., Daboussi, F., Thomas, S., Maréchal, A., Macmaster, R., Melliand, K., Juillerat, A., and Duchateau, P. (2012). Overcoming transcription activator-like effector (TALE) DNA binding domain sensitivity to cytosine methylation. J. Biol. Chem. *287*, 38427–38432.

38. Qasim, W., Zhan, H., Samarasinghe, S., Adams, S., Amrolia, P., Stafford, S., Butler, K., Rivat, C., Wright, G., Somana, K., et al. (2017). Molecular remission of infant B-ALL after infusion of universal TALEN gene-edited CAR T cells. Sci. Transl. Med. *9*, https://doi.org/10.1126/scitranslmed.aaj2013.

39. Gajewski, T.F., Schreiber, H., and Fu, Y.X. (2013). Innate and adaptive immune cells in the tumor microenvironment. Nat. Immunol. *14*, 1014–1022.

40. Zheng, Y., Zha, Y., and Gajewski, T.F. (2008). Molecular regulation of T-cell anergy. EMBO Rep. *9*, 50–55.

41. Beatty, G.L. (2014). Engineered chimeric antigen receptor-expressing T cells for the treatment of pancreatic ductal adenocarcinoma. OncoImmunology *3*, e28327.

42. Liu, X., Ranganathan, R., Jiang, S., Fang, C., Sun, J., Kim, S., Newick, K., Lo, A., June, C.H., Zhao, Y., and Moon, E.K. (2016). A chimeric switch-receptor targeting PD1 augments the efficacy of second-generation CAR T cells in advanced solid tumors. Cancer Res. *76*, 1578–1590.

43. Cherkassky, L., Morello, A., Villena-Vargas, J., Feng, Y., Dimitrov, D.S., Jones, D.R., Sadelain, M., and Adusumilli, P.S. (2016). Human CAR T cells with cell-intrinsic PD-1 checkpoint blockade resist tumor-mediated inhibition. J. Clin. Invest. *126*, 3130–3144.

44. Guo, J., Gaj, T., and Barbas, C.F., 3rd (2010). Directed evolution of an enhanced and highly efficient FokI cleavage domain for zinc finger nucleases. J. Mol. Biol. *400*, 96–107.

45. Miller, J.C., Holmes, M.C., Wang, J., Guschin, D.Y., Lee, Y.L., Rupniewski, I., Beausejour, C.M., Waite, A.J., Wang, N.S., Kim, K.A., et al. (2007). An improved zinc-finger nuclease architecture for highly specific genome editing. Nat. Biotechnol. *25*, 778–785.

46. Szczepek, M., Brondani, V., Büchel, J., Serrano, L., Segal, D.J., and Cathomen, T. (2007). Structure-based redesign of the dimerization interface reduces the toxicity of zinc-finger nucleases. Nat. Biotechnol. *25*, 786–793.

OMTN, Volume *9*

Supplemental Information

Fine and Predictable Tuning of TALEN Gene Editing Targeting for Improved T Cell Adoptive Immunotherapy

Anne-Sophie Gautron, Alexandre Juillerat, Valérie Guyot, Jean-Marie Filhol, Emilie Dessez, Aymeric Duclert, Philippe Duchateau, and Laurent Poirot

Supplementary tables

Sequences of off-site targets predicted in silico

Offtarget name	left_Sequence_With_Mismatches	right_Sequence_With_Mismatches	type
T3v1OS1	tctcttAgatAtgcAA	AGgcTgatcaaagTga	RR
T3v1OS2	tacctctgAgAAAcca	gcTcagatcCCagaga	LR
T3v1OS3	tctcttAAatctgcAc	CcgcaTCtcCaagaga	RR
T3v1OS4	taccCAGgtggggccT	AgTcccTGcagaggta	LL
T3v1OS5	taccGcGAtggggcca	TcTcaTCtcaaagaga	LR
T3v1OS6	taActAtgCAgggcca	ATgcTccacaAaggta	LL
T3v1OS7	tctctttgaGctTcAG	ATgcaTatcaTagaga	RR
T3v1OS8	tGcctcAgtgAggTca	CcAcagatTaaTgaga	LR
T3v1OS9	tacctctgtgTgAAcT	tggcccTacagagTGa	LL
T3v1OS10	tctctttAaActTcAc	tgTccccTcTgTggta	RL
T3v1OS11	tctctCAgaGctgcgc	CggccccacaTaCTta	RL
T3v1OS12	tacctctgCAggAcca	gcgcaCTGcaaCgaga	LR
T3v1OS13	tcAcCGtgatctgAgc	tggccAcGcagGTgta	RL
T3v1OS14	tGccGctgGggAgcca	GAgGcccaGagaggta	LL

Offtarget name	left_Sequence_With_Mismatches	right_Sequence_With_Mismatches	type	type
TRAC/T3v2OS1	tGcctctgCggAgcT	TgccccCTagaggta	PD1T3L	PD1T3L
TRAC/T3v2OS2	tcCctGGgatctgcA	Tgcagatcaaaga Ta	PD1T3R	PD1T3R
TRAC/T3v2OS3	tGcctcCAtggggcc	atCtctgtgTgTcCa	PD1T3L	TRAC_L
TRAC/T3v2OS4	tGccActgtggggAc	ggcccTGGTgaggCa	PD1T3L	PD1T3L
TRAC/T3v2OS5	tctcaActgAtacaG	TTcaTCtcaGagaga	TRAC_R	PD1T3R
TRAC/T3v2OS6	tctcttAgatAtgcA	GgcTgatcaaagTga	PD1T3R	PD1T3R
TRAC/T3v2OS7	ttgtAccacaAatat	cTTagGtcTCTgaga	TRAC_L	PD1T3R
TRAC/T3v2OS8	tctcAGAgaCctAAg	atatTtgtggTacaa	PD1T3R	TRAC_L
TRAC/T3v2OS9	tctcAGAgaCctAAg	atatTtgtggTacaa	PD1T3R	TRAC_L
TRAC/T3v2OS10	tctcAGAgaCctAAg	atatTtgtggTacaa	PD1T3R	TRAC_L
TRAC/T3v2OS11	ttgtAccacaAatat	cTTagGtcTCTgaga	TRAC_L	PD1T3R
TRAC/T3v2OS12	tctcAGAgaCctAAg	atatTtgtggTacaa	PD1T3R	TRAC_L
TRAC/T3v2OS13	tAtctttgaActgAg	CTccccTcagTggta	PD1T3R	PD1T3L
TRAC/T3v2OS14	ttgtccAaAagaCGt	cAcaTatcaTagaga	TRAC_L	PD1T3R
TRAC/T3v2OS15	tacctctCtAggAcc	TAcTgatTGaagaga	PD1T3L	PD1T3R
TRAC/T3v2OS16	taccAcAgAggggAc	cgTagCtcaaagTTa	PD1T3L	PD1T3R
TRAC/T3v2OS17	tGccActgtgggCAc	TgTagatcaGaTaga	PD1T3L	PD1T3R
TRAC/T3v2OS18	tctAtttgaActgAA	GGatTtgtTggacaa	PD1T3R	TRAC_L
TRAC/T3v2OS19	ttAGTcAacagatat	cgTagTtTaaagaga	TRAC_L	PD1T3R
TRAC/T3v2OS20	tctctttAatcAgAg	TTTagatcaTagaAa	PD1T3R	PD1T3R
TRAC/T3v2OS21	tctcttAAatctgcA	cgcaTCtcCaagaga	PD1T3R	PD1T3R
TRAC/T3v2OS22	tGcctctAAgAgAcc	cAcagatcTaagTga	PD1T3L	PD1T3R
TRAC/T3v2OS23	tGcctctgtgggCcc	cTTaAatcaGagaga	PD1T3L	PD1T3R
TRAC/T3v2OS24	tacctcGAAgggAAc	TTcaAatcaaagaga	PD1T3L	PD1T3R
TRAC/T3v2OS25	tGcctcAgtgAggTc	cAcagatTaaTgaga	PD1T3L	PD1T3R

List of oligonucleotides used for NGS sequencing to analyze off-target cleavages

T3v1OS1M1	CCATCTCATCCCTGCGTGTCTCCGACTCAGACGAGTGCGTGCTGAGCAGAACAGTCATGG
T3v1OS1M15	CCATCTCATCCCTGCGTGTCTCCGACTCAGATACGACGTAGCTGAGCAGAACAGTCATGG
T3v1OS2M2	CCATCTCATCCCTGCGTGTCTCCGACTCAGACGCTCGACAACGGCAGGAACTCCATTAGC
T3v1OS2M16	CCATCTCATCCCTGCGTGTCTCCGACTCAGTCACGTACTAACGGCAGGAACTCCATTAGC
T3v1OS3M3	CCATCTCATCCCTGCGTGTCTCCGACTCAGAGACGCACTCAGGATCATACTCTGCCACGC
T3v1OS3M17	CCATCTCATCCCTGCGTGTCTCCGACTCAGCGTCTAGTACAGGATCATACTCTGCCACGC
T3v1OS4M4	CCATCTCATCCCTGCGTGTCTCCGACTCAGAGCACTGTAGTCAGCTTAGGGCCTTTTCTCA
T3v1OS4M18	CCATCTCATCCCTGCGTGTCTCCGACTCAGTCTACGTAGCTCAGCTTAGGGCCTTTTCTCA
T3v1OS5M5	CCATCTCATCCCTGCGTGTCTCCGACTCAGATCAGACACGGCTAGGCAAGGGAGTATGGG
T3v1OS5M19	CCATCTCATCCCTGCGTGTCTCCGACTCAGTGTACTACTCGCTAGGCAAGGGAGTATGGG
T3v1OS6M6	CCATCTCATCCCTGCGTGTCTCCGACTCAGATATCGCGAGAGAACCTCAGAGAGCTACTGC
T3v1OS6M20	CCATCTCATCCCTGCGTGTCTCCGACTCAGACGACTACAGAGAACCTCAGAGAGCTACTGC
T3v1OS7M7	CCATCTCATCCCTGCGTGTCTCCGACTCAGCGTGTCTCTAACAGTGATTGTTTCTAGGTGGC
T3v1OS7M21	CCATCTCATCCCTGCGTGTCTCCGACTCAGCGTAGACTAGACAGTGATTGTTTCTAGGTGGC
T3v1OS8M8	CCATCTCATCCCTGCGTGTCTCCGACTCAGCTCGCGTGTCTCCATCACCTCTTGAGCATTTATCA
T3v1OS8M22	CCATCTCATCCCTGCGTGTCTCCGACTCAGTACGAGTATGTCCATCACCTCTTGAGCATTTATCA
T3v1OS9M9	CCATCTCATCCCTGCGTGTCTCCGACTCAGTAGTATCAGCACAGGAAAGAAACACACTGTTGG
T3v1OS9M23	CCATCTCATCCCTGCGTGTCTCCGACTCAGTACTCTCGTGACAGGAAAGAAACACACTGTTGG
T3v1OS10M10	CCATCTCATCCCTGCGTGTCTCCGACTCAGTCTCTATGCGAGGCGTGACTTCAATCATCCA
T3v1OS10M24	CCATCTCATCCCTGCGTGTCTCCGACTCAGTAGAGACGAGAGGCGTGACTTCAATCATCCA
T3v1OS11M11	CCATCTCATCCCTGCGTGTCTCCGACTCAGTGATACGTCTCGTATCCCCAGCGACTAAGC
T3v1OS11M25	CCATCTCATCCCTGCGTGTCTCCGACTCAGTCGTCGCTCGCGTATCCCCAGCGACTAAGC
T3v1OS12M12	CCATCTCATCCCTGCGTGTCTCCGACTCAGTACTGAGCTACGGGAGCTTCACTGAGTCAC
T3v1OS12M26	CCATCTCATCCCTGCGTGTCTCCGACTCAGACATACGCGTCGGGAGCTTCACTGAGTCAC
T3v1OS13M13	CCATCTCATCCCTGCGTGTCTCCGACTCAGCATAGTAGTGCCCCTTCCTAGCCATGAATGA
T3v1OS13M27	CCATCTCATCCCTGCGTGTCTCCGACTCAGACGCGAGTATCCCCTTCCTAGCCATGAATGA
T3v1OS14M14	CCATCTCATCCCTGCGTGTCTCCGACTCAGCGAGAGATACTACGTCATAACACTGCGCGGCC
T3v1OS14M28	CCATCTCATCCCTGCGTGTCTCCGACTCAGACTACTATGTTACGTCATAACACTGCGCGGCC
T3v1OS1R	CCTATCCCCTGTGTGCCTTGGCAGTCTCAGGAGTGTCACTCTGGAGGGCA
T3v1OS2R	CCTATCCCCTGTGTGCCTTGGCAGTCTCAGAGGCTTGGCTAGATCTGGGA
T3v1OS3R	CCTATCCCCTGTGTGCCTTGGCAGTCTCAGAGCTGAATTTTTCTCGGGCA
T3v1OS4R	CCTATCCCCTGTGTGCCTTGGCAGTCTCAGCAGTCCTCTTCCCTCACTTGG
T3v1OS5R	CCTATCCCCTGTGTGCCTTGGCAGTCTCAGGACTCTACTCCTGGATCCCCA
T3v1OS6R	CCTATCCCCTGTGTGCCTTGGCAGTCTCAGACCACCCTCTGTTTGTCTCAG
T3v1OS7R	CCTATCCCCTGTGTGCCTTGGCAGTCTCAGAGCAGTCATCTCCTGGAGCC
T3v1OS8R	CCTATCCCCTGTGTGCCTTGGCAGTCTCAGTCATTTGCAGCAACACAGATGG
T3v1OS9R	CCTATCCCCTGTGTGCCTTGGCAGTCTCAGGGCACAAACCTTCTTCAAGTAGA
T3v1OS10R	CCTATCCCCTGTGTGCCTTGGCAGTCTCAGCTGAAAGTCACCCCTGCACC
T3v1OS11R	CCTATCCCCTGTGTGCCTTGGCAGTCTCAGCTTATCACCCGGAACCTGCA
T3v1OS12R	CCTATCCCCTGTGTGCCTTGGCAGTCTCAGTGGAGCCTCACCATAGGGAC
T3v1OS13R	CCTATCCCCTGTGTGCCTTGGCAGTCTCAGTCTCCATCCTGCCCATGAGC
T3v1OS14R	CCTATCCCCTGTGTGCCTTGGCAGTCTCAGGGTTGGAGTTGCTTCTCGGA
T3v1MIDF25	CCATCTCATCCCTGCGTGTCTCCGACTCAGTCGTCGCTCGGACAGAGATGCCGGTCACCATTC
T3v1MIDF26	CCATCTCATCCCTGCGTGTCTCCGACTCAGTCGTCGCTCGGACAGAGATGCCGGTCACCATTC
T3v1MIDR	CCTATCCCCTGTGTGCCTTGGCAGTCTCAGGGACAACGCCACCTTCACCTGC

TRAC/T3v2OS1F	AAGACTCGGCAGCATCTCCATTGAGGCATATTCGGGCAGG
TRAC/T3v2OS1-1R	GCGATCGTCACTGTTCTCCAGGCCCTAACTCAAACCCACA
TRAC/T3v2OS2-F	AAGACTCGGCAGCATCTCCATGACTTTGTAGCTCCCTCTGC
TRAC/T3v2OS2-R	GCGATCGTCACTGTTCTCCATAACCTAGGCACATCCTCCC
TRAC/T3v2OS3-1-F	AAGACTCGGCAGCATCTCCATGCACCACAGAACTGGGTGA
TRAC/T3v2OS3-1-R	GCGATCGTCACTGTTCTCCAGGCTTTAATCCAGGATGACTGC
TRAC/T3v2OS4-1-F	AAGACTCGGCAGCATCTCCATTCTTAGCACAGGGCCTTGG
TRAC/T3v2OS4-1-R	GCGATCGTCACTGTTCTCCAGACCTGGCTCGTTTCTGTGA
TRAC/T3v2OS5-1-F	AAGACTCGGCAGCATCTCCAAAACCCTGGCCACATCTTCA
TRAC/T3v2OS5-1-R	GCGATCGTCACTGTTCTCCAACCTCATGGTCGCAAAGTGG
TRAC/T3v2OS6-1-F	AAGACTCGGCAGCATCTCCAAGTTAGGGGAGGCAGGGAGA
TRAC/T3v2OS6-1-R	GCGATCGTCACTGTTCTCCAACAGCCCCGCTTTCTATCCC
TRAC/T3v2OS7-1-F	AAGACTCGGCAGCATCTCCATGAAAAATGAGGAAGGGTGCC
TRAC/T3v2OS7-1-R	GCGATCGTCACTGTTCTCCATCCATGACAACTCTGAGTTAGCA
TRAC/T3v2OS8-2-F	AAGACTCGGCAGCATCTCCATCCTATATAATGCCAGATTAGC
TRAC/T3v2OS8-2-R	GCGATCGTCACTGTTCTCCATGAAAGATGAGGAAGAGTGC
TRAC/T3v2OS13-F	AAGACTCGGCAGCATCTCCAATGGACATAAATTTAAGCTAGCAGC
TRAC/T3v2OS13-R	GCGATCGTCACTGTTCTCCAGCCCTTACACATGTTCTTGCA
TRAC/T3v2OS14-F	AAGACTCGGCAGCATCTCCATGGGGGAGTTACAGAAAGCC
TRAC/T3v2OS14-R	GCGATCGTCACTGTTCTCCACTGATGGAATTACAGGCATAGCA
TRAC/T3v2OS15-1-F	AAGACTCGGCAGCATCTCCAGCAAGTCAGTCATTTGTCAGGG
TRAC/T3v2OS15-1-R	GCGATCGTCACTGTTCTCCATACTATTCGGGAGCGCAGGA
TRAC/T3v2OS16-1-F	AAGACTCGGCAGCATCTCCACCCCTTCTCTTCTTCCCTCC
TRAC/T3v2OS16-1-R	GCGATCGTCACTGTTCTCCACATGGTGAGTACTCAGGCCA
TRAC/T3v2OS17-1-F	AAGACTCGGCAGCATCTCCAGCCCATAAAATGCCCAAGCC
TRAC/T3v2OS17-1-R	GCGATCGTCACTGTTCTCCAAAGAGGTCAGAGTCTGGGCA
TRAC/T3v2OS18-1-F	AAGACTCGGCAGCATCTCCATTGACTCTGTGCCAGGAACC
TRAC/T3v2OS18-1-R	GCGATCGTCACTGTTCTCCAAGGAGAGGAGAGGACCTGGA
TRAC/T3v2OS19-1-F	AAGACTCGGCAGCATCTCCACAGAAAGAGAGAGGAGAAAGAAAGA
TRAC/T3v2OS19-1-R	GCGATCGTCACTGTTCTCCACATGGAACTTCTTTCTGGTCTCC
TRAC/T3v2OS20-1-F	AAGACTCGGCAGCATCTCCAGCCTTTCTCCTGAGCTGTGA
TRAC/T3v2OS20-1-R	GCGATCGTCACTGTTCTCCAGCTGCAACAATGGTTTACTTTGC
TRAC/T3v2OS21-1-F	AAGACTCGGCAGCATCTCCAAGCACTTCACTTAACTCAGGATCA
TRAC/T3v2OS21-1-R	GCGATCGTCACTGTTCTCCAAAATGAGATGATACCTCTTCTGACC
TRAC/T3v2OS22-1-F	AAGACTCGGCAGCATCTCCAGGCATCCTTCCATCAGCACA
TRAC/T3v2OS22-1-R	GCGATCGTCACTGTTCTCCATGCACAATTCTTTTTAACACACGC
TRAC/T3v2OS23-F	AAGACTCGGCAGCATCTCCATGTCTAGATGGGAATGGTTTGC
TRAC/T3v2OS23-R	GCGATCGTCACTGTTCTCCAGCCCATGATTTTCTTCCATAGTCA
TRAC/T3v2OS25-2-F	AAGACTCGGCAGCATCTCCATGTATGTTTGTACCTTTTAGCCAAC
TRAC/T3v2OS25-2-R	GCGATCGTCACTGTTCTCCAACTGAAGCACTGTTCACCATAG

Total number of reads and total number of events detected, Figure 2C

Non-transfected			
Target	# Evts	# total reads	estimated indels frequency
PD-1	0	5898	< 0.000170
off-site #1	0	11234	< 0.000089
off-site #2	0	1364	< 0.000733
off-site #3	0	15178	< 0.000066
off-site #4	0	15043	< 0.000066
off-site #5	0	10077	< 0.000099
off-site #6	0	33787	< 0.000030
off-site #7	0	10778	< 0.000093
off-site #8	0	4133	< 0.000242
off-site #9	3	12554	0.000239
off-site #10	0	13595	< 0.000074
off-site #11	0	13689	< 0.000073
off-site #12	21	9066	0.002316
off-site #13	0	5675	< 0.000176
off-site #14	0	2399	< 0.000417

T3v1 PD-1			
Target	# Evts	# total reads	estimated indels frequency
PD-1	3388	3678	0.921153
off-site #1	0	10714	< 0.000093
off-site #2	0	1990	< 0.000503
off-site #3	0	9304	< 0.000107
off-site #4	0	15664	< 0.000064
off-site #5	0	12330	< 0.000081
off-site #6	2	43075	0.000046
off-site #7	0	12146	< 0.000082
off-site #8	0	3488	< 0.000287
off-site #9	244	20926	0.011660
off-site #10	0	15634	< 0.000064
off-site #11	0	16972	< 0.000059
off-site #12	10	10185	0.000982
off-site #13	0	2126	< 0.000470
off-site #14	3	3889	0.000771

The efficiency of T3v1 PD-1 TALEN-mediated gene processing was analyzed by high-throughput DNA sequencing analysis using 454 sequencing system. The indels frequency is estimated as followed: total number of events/total number of reads.

Total number of reads and total number of events detected, Figure 3C

Non-transfected			
Target	# Evts	# total reads	estimated indels frequency
PD-1	1	4356	0.00022957
off-site #9	1	14080	7.1023E-05

T3v2 PD-1			
Target	# Evts	# total reads	estimated indels frequency
PD-1	4141	4559	0.90831323
off-site #9	0	11223	< 0.000089

T3v3 PD-1			
Target	# Evts	# total reads	estimated indels frequency
PD-1	4010	4780	0.83891213
off-site #9	1	4691	0.00021317

The efficiency of T3v2 and T3v3 PD-1 TALEN-mediated gene processing was analyzed by high-throughput DNA sequencing analysis using 454 sequencing system. The indels frequency is estimated as followed: total number of events/total number of reads.

Total number of reads and total number of events detected, Figure 4A

Non-transfected			
Target	# Evts	# total reads	estimated indels frequency
PD-1	14	9703	0.001443
TRAC	5	15331	0.000326
off-site #1	1	6727	0.000149
off-site #2	1	9173	0.000109
off-site #3	0	9167	< 0.000109
off-site #4	6	11614	0.000517
off-site #5	0	4584	< 0.000218
off-site #6	0	4157	< 0.000241
off-site #7	4	16037	0.000249
off-site #8	0	16669	< 0.00006
off-site #13	5	15147	0.000330
off-site #14	0	8797	< 0.000114
off-site #15	698	15287	0.045660
off-site #16	1	18109	0.000055
off-site #17	17	9861	0.001724
off-site #18	2	6052	0.000330
off-site #19	3	11415	0.000263
off-site #20	4	8167	0.000490
off-site #21	0	2065	< 0.000484
off-site #22	4	11239	0.000356
off-site #23	8	10088	0.000793
off-site #24	1	5271	0.000190
off-site #25	45	14415	0.003122

T3v2 PD-1/TRAC			
Target	# Evts	# total reads	estimated indels frequency
PD-1	5539	7059	0.784672
TRAC	9	6190	0.001454
off-site #1	6	12799	0.000469
off-site #2	248	8371	0.029626
off-site #3	1	10716	0.000093
off-site #4	0	4330	< 0.000231
off-site #5	0	4167	< 0.000537
off-site #6	7	13040	0.000537
off-site #7	1	14157	0.000071
off-site #8	7	16926	0.000414
off-site #13	1	12087	0.000083
off-site #14	736	15230	0.048326
off-site #15	1	15038	0.000066
off-site #16	24	12413	0.001933
off-site #17	1	5793	0.000173
off-site #18	1	12288	0.000081
off-site #19	3	8184	0.000367
off-site #20	1	2804	0.000357
off-site #21	2	12478	0.000160
off-site #22	6	8545	0.000702
off-site #23	1	7096	0.000141
off-site #24	18	12156	0.001481
off-site #25	3933	8911	0.441365

In depth characterization of the molecular events generated by T3v2 PD-1 TALEN in combination with TRAC TALEN by high-throughput DNA sequencing analysis using Illumina method. The indels frequency is estimated as followed: total number of events/total number of reads.

Total number of reads and total number of events detected, Figure 4C

Non-transfected			
Target	# Evts	# total reads	estimated indels frequency
PD-1	265	78440	0.003378378
TRAC	412	184080	0.002238157
v2OS3	6	95819	6.26181E-05
v1OS9	51	135931	0.00037519

T3v1 PD-1/TRAC			
Target	# Evts	# total reads	estimated indels frequency
PD-1	60009	67419	0.890090331
TRAC	61559	100579	0.612046252
v2OS3	2553	97569	0.026166098
v1OS9	1762	128743	0.013686181

T3v2 PD-1/TRAC			
Target	# Evts	# total reads	estimated indels frequency
PD-1	65292	71167	0.917447693
TRAC	72287	113150	0.63885992
v2OS3	1520	101328	0.01500079
v1OS9	73	148720	0.000490855

T3v3 PD-1/TRAC			
Target	# Evts	# total reads	estimated indels frequency
PD-1	80010	92730	0.862827564
TRAC	53601	107114	0.500410777
v2OS3	747	104308	0.007161483
v1OS9	58	129894	0.000446518

T3v4 PD-1/TRAC			
Target	# Evts	# total reads	estimated indels frequency
PD-1	54533	73740	0.739530784
TRAC	52627	89848	0.585733684
v2OS3	11	133406	8.24551E-05
v1OS9	47	140867	0.000333648

In depth characterization of the molecular events generated by T3v1, T3v2, T3v3 or T3v4 PD-1 TALEN in combination with TRAC TALEN by high-throughput DNA sequencing analysis using Illumina method. The indels frequency is estimated as followed: total number of events/total number of reads.